

${}^6,{}^7\text{Li}(\pi^+, \text{pd}){}^3,{}^4\text{He}$ reactions at 59.4 MeV

W. R. Wharton

Wheaton College, Wheaton, Illinois 60187

P. D. Barnes, B. Bassalleck,* R. A. Eisenstein,† G. Franklin, R. Grace,
C. Maher, P. Pile,‡ R. Rieder,§ and J. Szymanski
Carnegie-Mellon University, Pittsburgh, Pennsylvania 15213

F. Takeuchi

Kyoto-Sangyo University, Kyoto 603, Japan

J. F. Amann

Los Alamos Scientific Laboratory, Los Alamos, New Mexico 87545

S. A. Dytman

University of Pittsburgh, Pittsburgh, Pennsylvania 15213

K. G. R. Doss**

University of Washington, Seattle, Washington 98195

(Received 26 December 1985)

The (π^+, pd) reactions on ${}^6\text{Li}$ and ${}^7\text{Li}$ have been studied at $T_\pi = 59.4$ MeV. Triple- and single-differential cross sections for these reactions are presented. The data are fitted to a T matrix and compared to the ${}^3\text{H}(\pi^+, \text{p}){}^2\text{H}$ reaction. A model in which the pion interacts and is absorbed on a "quasi-triton" cluster describes the main features of the data very well. An extrapolation of our data into unmeasured regions of phase space suggests that about 8% of the pion absorption cross section on ${}^6\text{Li}$ at 59.4 MeV goes into the (π^+, pd) channel. The ${}^7\text{Li}(\pi^+, \text{pd}){}^4\text{He}(2^-)$ transition at 22.1 MeV excitation appears to be strongly populated. This is a surprise because it is not seen in the ${}^7\text{Li}(\text{p}, \alpha){}^4\text{He}$ reaction.

I. INTRODUCTION

The mechanisms by which pions are absorbed in nuclei are still poorly understood.¹ We have only an imprecise knowledge of the extent to which more than two nucleons are directly involved in the absorption process and the mechanism by which these nucleons become involved. The purpose of this report is to present a detailed study of the ${}^6,{}^7\text{Li}(\pi^+, \text{pd}){}^3,{}^4\text{He}$ reaction at 59.4 MeV to learn about the reaction mechanism for pion absorption on three nucleons.

The lithium isotopes have $1p$ -shell nucleons clustered into a quasi-deuteron or quasi-triton and loosely bound to a $(1s)^4$ alphas core. In a recent paper,² we published data on the ${}^6,{}^7\text{Li}(\pi^+, 2\text{p}){}^4,{}^5\text{He}$ reaction at $T = 59.4$ MeV. The data were well described by a model in which the pion is absorbed on a 3S_1 $\langle \text{pn} \rangle$ "quasi-deuteron" cluster leaving the other $A-2$ nucleons undisturbed. For example, the ${}^6\text{Li}(\pi^+, \text{pp}){}^4\text{He}(\text{g.s.})$ transition showed a recoil momentum distribution identical (within errors) to the ${}^6\text{Li}(\text{e}, \text{e}'\text{d})$ and ${}^6\text{Li}(\text{p}, \text{pd})$ deuteron knockout reactions. Also, the ${}^6\text{Li}(\pi^+, \text{pp}){}^4\text{He}(\text{g.s.})$ single-differential cross section was nearly identical in magnitude, angular distribution, and energy dependence to the elementary $\pi^+ + \text{d} \rightarrow \text{p} + \text{p}$ cross section. These results indicate that the $(1s)^4$ core of the lithium nuclei had no noticeable involvement in the pion

absorption with the p -shell nucleons. Transitions in which a pion was absorbed on quasi-deuteron-like clusters involving $(1s)^4$ core nucleons in the lithium nuclei also showed similarities with the elementary $\pi^+ + \text{d} \rightarrow \text{p} + \text{p}$ reaction.

In this paper, the ${}^6,{}^7\text{Li}(\pi^+, \text{pd}){}^3,{}^4\text{He}$ reaction will be studied in a similar fashion to see how well it is described by a model in which the pion is absorbed on a $\langle \text{pnn} \rangle$ "quasi-triton" cluster. In this model the three nucleons are directly involved in the pion annihilation process and the $\text{Li}(\pi^+, \text{pd})$ cross section is similar to the elementary ${}^3\text{H}(\pi^+, \text{p}){}^2\text{H}$ reaction. This single step process can be easily distinguished from the two-step process, $(\pi^+, \text{p}_1\text{p}_2)$ followed by a neutron pickup (p_2, d) in which the intermediate proton, p_2 , is nearly on shell, since this two-step process would have very different kinematics from a triton-cluster annihilation.³

In our earlier ${}^6,{}^7\text{Li}(\pi^+, 2\text{p}){}^3,{}^4\text{He}$ paper we reported that an extrapolation of our data into unmeasured regions using the successful "quasi-deuteron" model indicated that about 60% of the pion absorption cross section on ${}^6\text{Li}$ at 59.4 MeV goes into the (π^+, pp) channel. We also gave evidence that this fraction decreases to about 30% at $T_\pi = 160$ MeV. As the "quasi-triton" model is successful for the $\text{Li}(\pi^+, \text{pd})$ reactions we will also make a similar extrapolation for these reactions to estimate the fraction

of the total pion absorption cross section going into the (π^+,pd) channels.

II. EXPERIMENTAL AND DATA REDUCTION OVERVIEWS

The ${}^6,{}^7\text{Li}(\pi^+,pd){}^3,{}^4\text{He}$ data at 59.4 MeV at $\theta_p=60^\circ$, 80.5° , and 102.7° were taken simultaneously with the $\text{Li}(\pi^+,pp)$ data² and our published $\text{Li}(\pi^+,HeHe)$ and $\text{Li}(\pi^+,Het)$ data.⁴ The experimental setup in the LEP channel at LAMPF and the analysis procedure is well described in these two papers and also in a paper on our ${}^{16}\text{O}(\pi^+,pp)$ data.⁵ Hence, we only give a brief description of the procedure here. The direction of motion and the energy of the two charged particles in coincidence were detected using multiwire proportional chambers followed by solid-state spectrometers made with high purity germanium crystals and two Si(Li) crystals. This is a kinematically complete experiment for a three-body final state, allowing us to determine the total energy (missing mass) and total momentum (recoil momentum) of the third undetected particle. Two ionization chambers downstream of the target monitored the intensity of the incident beam. The targets had thicknesses of either 100 or 150 mg/cm² of ${}^6\text{Li}$ enriched to 95.6% and 150 mg/cm² of ${}^7\text{Li}$ enriched to 99.9%. The energy threshold for identifying protons and deuterons by dE/dx measurements in our spectrometers was about 32 and 42 MeV, respectively. The effective threshold is higher due to the energy straggling losses in the target, etc. One of the spectrometers (with four crystals) had a thickness corresponding to the range of a 120 MeV proton. This was adequate for the $\text{Li}(\pi^+,pp)$ reactions but inadequate for the $\text{Li}(\pi^+,pd)$ reactions which have a continuous distribution of proton energies up to about 145 MeV. Fortunately we were able to identify and determine accurately the energy of the protons passing through the last crystal in this spectrometer. Using the measured dE/dx in the four crystals and the known energy dependence of the proton's dE/dx , we were able to identify these proton "nonstops" and estimate their total energy. Figure 1 shows a dot plot of the total energy which protons deposit in the spectrometer with the energy deposited in the last crystal. The proton "non-

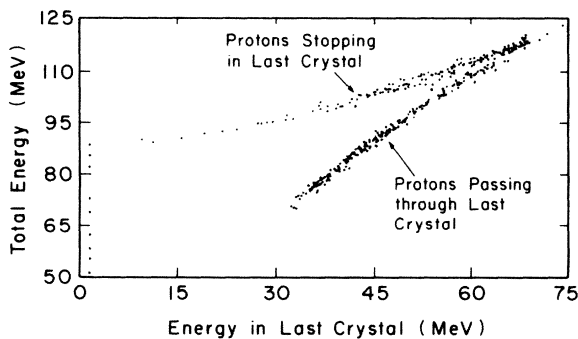


FIG. 1. A dot plot of all particles in the four crystal spectrometer which leave between 5.1 and 6.6 MeV in the second crystal and between 29 and 38 MeV in the third crystal.

stops" are clearly identified as events within a narrow band labeled in the figure. Once identified as "nonstop" protons, the actual unmeasured total energy of these particles is reconstructed. The energy resolution of the reconstructed energy is limited by energy straggling in the crystals to about 3.0 MeV. This is shown in Fig. 2 as a missing mass spectrum for nonstop protons in the ${}^7\text{Li}(\pi^+,pd){}^4\text{He}$ reaction. For events in which the protons are stopped the resolution is typically 2.4 MeV, being limited by energy straggling in the Li targets. Typical missing mass spectra for stopped protons are shown in Figs. 3 and 4.

The analysis of the data involves a Monte Carlo simulation of the nuclear reactions and experimental detection system. This is described in detail elsewhere.^{2,4,5} The procedure leads to the extraction of triple-differential cross sections. One such cross section is expressed as:

$$\frac{d^3\sigma}{dE_p d\Omega_p d\Omega_d} = \frac{1}{(2\pi)^5} \frac{E_\pi E_p E_d k_p k_d}{k_\pi |1 - (\boldsymbol{\beta}_R \cdot \boldsymbol{\beta}_d) / \beta_d^2|} |T|^2, \quad (1)$$

where the kinematic factor includes energies, wave numbers, and velocities of the two detected particles (subscripts p and d) and the recoiling nucleus (subscript R). The transition matrix, T , is sensitive to the initial and final wave function of Li and He, respectively, and the precise nature of the reaction mechanism. Since there are three particles in the final state, nine coordinates are needed to specify the kinematics of each event, reduced to five by conservation of energy and momentum. The Monte Carlo code used the five variables: \mathbf{P}_R , the momentum of the recoiling nucleus, and θ_p, ϕ_p , the angles of the proton. The angles, θ_p, ϕ_p , are defined as the angles between the detected proton and the incident pion momentum direction with ϕ_p as the azimuthal angle. These variables are chosen for reasons which simplify the data analysis. The angles θ_p and ϕ_p are chosen because they are constrained to a small range of values during a single experimental run. The T matrix is expected to depend strongly upon the recoil momentum, $\mathbf{P}_R = \mathbf{P}_\pi - \mathbf{P}_p - \mathbf{P}_d$. In the impulse approximation and quasi-triton model, $-\mathbf{P}_R$ is also the total momentum of the three nucleons on which the pion is absorbed. The goal of the Monte Carlo code is to find the ${}^6,{}^7\text{Li}(\pi^+,pd){}^3,{}^4\text{He}$ T -matrix dependence of four of the above five variables, as the T matrix should be indepen-

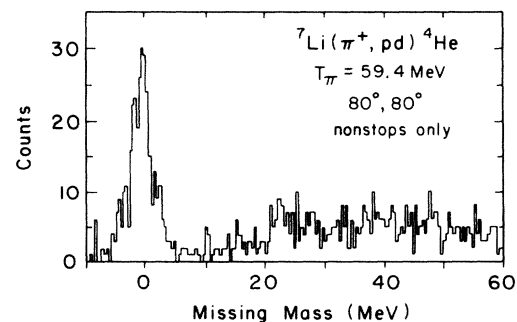


FIG. 2. ${}^7\text{Li}(\pi^+,pd){}^4\text{He}$ missing mass spectrum for nonstop protons in the four crystal spectrometer.

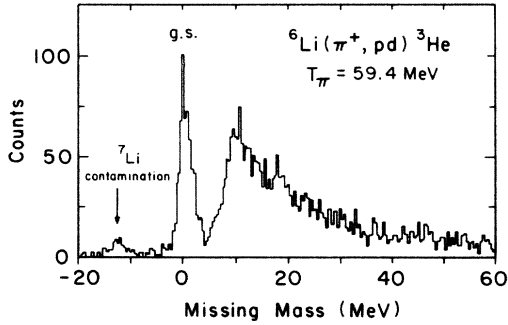


FIG. 3. A ${}^6\text{Li}(\pi^+, \text{pd}){}^3\text{He}$ missing mass spectrum.

dent of ϕ_p due to cylindrical symmetry. The advantage of using a procedure involving a T matrix is that it succinctly summarizes the information contained in the five-dimensional space, which would be hard to display graphically. It was found that a choice of $|T(\theta_p, P_R)|^2$ based upon the quasi-triton model successfully described the experimental data. This successful functional form is

$$|T|^2 = f(P_R)G(\theta'_p), \quad (2)$$

where P_R is the momentum of the residual nucleus and $G(\theta'_p)$ is the known measured angular distribution of the ${}^3\text{H}(\pi^+, \text{p}){}^2\text{H}$ reaction; the prime designates that θ'_p is measured in the $p + d$ center-of-mass reference frame. $f(P_R)$ is expressed in the laboratory frame in which the target is at rest. In the quasi-triton model $f(P_R)$ is a form factor describing the motion of the quasi-triton as an elementary particle with respect to the target nucleus. In the plane-wave Born approximation there is no preferred direction and the T matrix is independent of the direction of P_R .

The Monte Carlo code uses this functional form for the T matrix to simulate the reaction and its detection by our apparatus. Both $f(P_R)$ and $G(\theta'_p)$ have an arbitrary functional form which is adjusted until all of the distributions from the Monte Carlo simulation agree with the data. In actuality, the yield distributions at a single set of detector angles were consistent with any reasonable functional form of $G(\theta'_p)$. Therefore, the choice of $G(\theta'_p)$ was not critical to the analysis procedure, and only at the end of the analysis did we carefully examine the $G(\theta'_p)$ dependence (see Sec. IV).

After the T matrix is adjusted to reproduce the data for a particular transition, it can be normalized using the

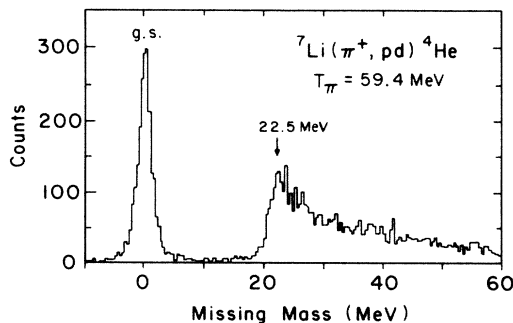


FIG. 4. A ${}^7\text{Li}(\pi^+, \text{pd}){}^4\text{He}$ missing mass spectrum.

detection efficiency calculated with the Monte Carlo code and the known ${}^6\pi^+d \rightarrow pp$ cross sections at 59.4 MeV,

$$d\sigma/d\Omega = (6.85/2\pi)[1 + 1.09P_2(\cos\theta')] \text{ mb/sr},$$

measured in the center-of-mass frame. At various times in the experiment, data were collected on the $\pi^+d \rightarrow pp$ process using a 194 mg/cm^2 CD_2 target and detecting both protons in coincidence. This was necessary to obtain absolute cross sections because the ionization chambers measuring the beam intensity did not take into account the impurity of the beam. The CD_2 runs, interspersed throughout the experiment, not only provided a calibration but also confirmed that the beam impurity was constant during the full experiment. The Monte Carlo code was used to calculate the detection efficiency of the $\pi^+d \rightarrow pp$ coincidence measurements. Any systematic errors in the Monte Carlo simulation which affect the calculated detection efficiencies of the $\pi^+d \rightarrow pp$ reaction and $\text{Li}(\pi^+, \text{pd})$ reactions equally, would cancel out in the normalization procedure. The $\pi^+d \rightarrow pp$ data also provided other valuable information (see Refs. 2 and 5 for details).

This is the last of our papers²⁻⁵ on the pion absorption charged particle coincidence measurements. The three sets of data reported in Refs. 2, 3, and 5 have absolute cross sections, which came from the same normalization procedures. There should be no more than a 10% systematic error in the relative absolute cross sections among any two sets of these data. Folded into this 10% is the uncertainty in the ${}^2\text{H}(\pi^+, \text{p}){}^2\text{H}$ cross sections, perhaps 10% also. The $\text{Li}(\pi^+, \text{HeHe})$ data⁴ used a different set of ${}^2\text{H}(\pi^+, \text{p})$ data for normalization, and an error in the analysis of that data gave an additional overestimate of the cross section by 22%. To make these analyzed cross sections in Ref. 4 consistent with the analysis in our more recent publications all reported cross sections in Refs. 4 at $T_\pi = 59.3 \text{ MeV}$ should be multiplied by 0.61 and at $T_\pi = 30 \text{ MeV}$ by the factor 0.68.

III. SPECTRA AND FORM FACTORS

Figure 3 shows a missing mass spectrum for the reaction ${}^6\text{Li}(\pi^+, \text{pd}){}^3\text{He}$. It is characterized by a peak at 0 MeV and a much broader enhancement starting at 5 MeV. The 0 MeV peak is the transition to the ground state, the only known stable state in ${}^3\text{He}$. This corresponds to the removal of the two p -shell nucleons and an s -shell nucleon. The remaining yield is thought to be due to four- and five-body final states since ${}^3\text{He}$ is unstable to $n + d$ decay at 5.5 MeV and to $n + p + p$ decay at 7.7 MeV. However, we will treat this as yield for a transition to a three-body state in which the proton and deuteron leave the residual nucleus in a temporarily unified, although unstable state.

Figure 4 displays a missing mass spectrum for the reaction ${}^7\text{Li}(\pi^+, \text{pd}){}^4\text{He}$. The strong ground state peak corresponds to the removal of the three p -shell nucleons which are well described as a "triton cluster." There is also considerable enhancement starting at 20 MeV corresponding to a region containing many known excited states of ${}^4\text{He}$. One excited state near 22 MeV appears to be enhanced

above the others. If we choose only the events with recoil momentum less than 60 MeV/c, the spectrum in Fig. 5 is obtained. Here, the state at 22.4 ± 0.4 MeV is almost as strong as the ground state transition. It is very likely that this is the known 2^- state at 22.1 MeV which is believed to be a (s^3p') configuration (i.e., one hole in the s shell and one nucleon in the p shell). This state is also one of the strongest excited states populated in the ${}^6\text{Li}(\pi^+, \text{pp}){}^4\text{He}$ reaction.²

It is interesting that this 22.1 MeV 2^- state is seen so strongly in the ${}^7\text{Li}(\pi^+, \text{pd}){}^4\text{He}$ reaction because there is absolutely no indication⁷ of it in the ${}^7\text{Li}(p, \alpha){}^4\text{He}$ spectra at $T_p = 9.1$ MeV. If both the (p, α) and (π^+, pd) reactions favor the removal of a (pnn) cluster with the internal quantum numbers of a triton, then the strongest states in both spectra should be identical, unless there is some other selection rule coming into play. In a separate measurement, we have found the ${}^{16}\text{O}(\pi^+, \text{pd}){}^{13}\text{N}$ and ${}^{16}\text{O}(p, \alpha){}^{13}\text{N}$ spectra to be similar, both populating the $\frac{3}{2}^-$ 3.5 MeV state and $\frac{1}{2}^-$ ground state of ${}^{13}\text{N}$ with a 2.5:1 ratio. Therefore, this suggests that there is something else involved in the ${}^4\text{He}$ (22.1 MeV) 2^- transition.

A plausible explanation for the difference between the (p, α) and (π^+, pd) reactions is that the former is more of a surface reaction and is more likely to disturb the remaining $(A-3)$ nucleons of the residual nucleus. We propose that the ${}^7\text{Li}(\pi^+, \text{pd}){}^4\text{He}^*$ (22.1 MeV) transition involves the removal of three nucleons from the $(1s)^4$ core leading to a $(1s1p^3)$ configuration. However, because of the ambiguity due to spurious center-of-mass motion it is possible to redefine the $1p^3$ nucleons as $1s^3$ nucleons and the $1s$ nucleon as a $1p$ nucleon thereby leading to the known

$(1s^31p)$ configuration of the 22.1 MeV 2^- state. The ${}^7\text{Li}(p, \alpha)$ reaction cannot populate this state because it cannot easily interact with the $(1s)^4$ core without disturbing the other nucleons.

To simplify our analysis we did not try to separate the 22.1 MeV state from the yield to surrounding ${}^4\text{He}$ excited states. Part of this yield in the excited state region is also due to four, five, and six particle-final states in the ${}^7\text{Li}(\pi^+, \text{pd})$ reaction. This is because ${}^4\text{He}$ is unbound to proton decay above 19.8 MeV excitation and can completely separate into two neutrons and two protons above 28.3 MeV. We chose to analyze the region from 17 to 42 MeV excitation in ${}^4\text{He}$ with a common T matrix even though a comparison of Figs. 4 and 5 shows that this is, strictly speaking, incorrect. These figures show that the 22.1 MeV 2^- state has a stronger yield at small recoil momentum than the surrounding states and continuum. However, the approximation of choosing a common T matrix should not significantly affect the extraction of cross sections given later in this paper. We also treat the excitation region 5 \rightarrow 30 MeV in the ${}^6\text{Li}(\pi^+, \text{pd}){}^3\text{He}$ reaction with a common T matrix.

The recoil momentum distribution, $f(P_R)$ in Eq. (2), for the four cases: ${}^4\text{He}$ ground state, ${}^4\text{He}^*$ (17 \rightarrow 42 MeV), ${}^3\text{He}$ ground state, and ${}^3\text{He}$ (5 \rightarrow 30 MeV) are shown in Figs. 6 and 7. These recoil momentum distributions were found to be independent of the proton angle θ_p . The central detector angles for protons were 60° , 80.5° , and 102.7° for the ${}^7\text{Li}(\pi^+, \text{pd})$ reaction and 60° and 102.7° for the ${}^6\text{Li}(\pi^+, \text{pd})$ reaction. The form factors are grouped together according to their similar shapes. In Fig. 6 the ${}^7\text{Li}(\pi^+, \text{pd}){}^4\text{He}(\text{g.s.})$ and ${}^6\text{Li}(\pi^+, \text{pd}){}^3\text{He}^*$ (5 \rightarrow 30 MeV)

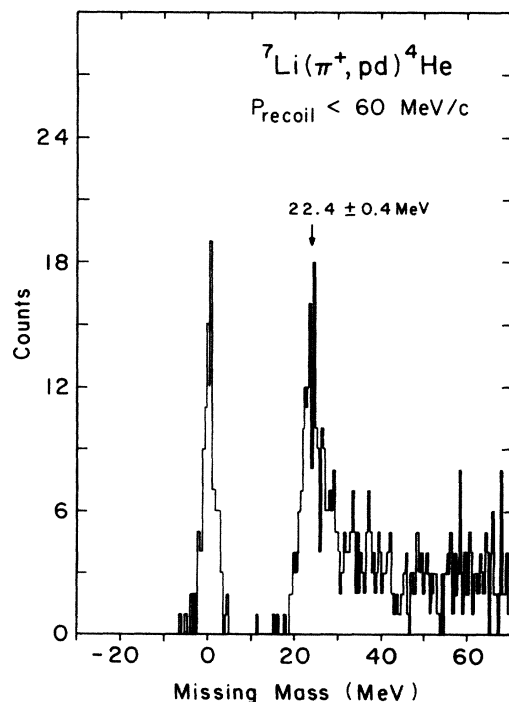


FIG. 5. A ${}^7\text{Li}(\pi^+, \text{pd}){}^4\text{He}$ missing mass spectrum for events with missing momentum, P_R , less than 60 MeV/c.

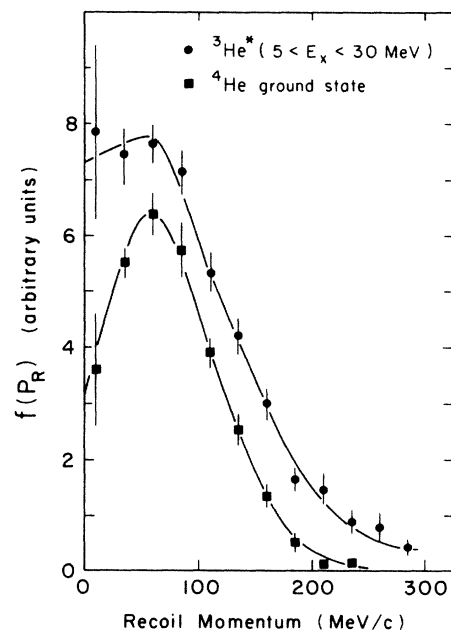


FIG. 6. The form factor, $f(P_R)$, in Eq. (2) for the ${}^7\text{Li}(\pi^+, \text{pd}){}^4\text{He}(\text{g.s.})$ and ${}^6\text{Li}(\pi^+, \text{pd}){}^3\text{He}^*$ (5 \rightarrow 30 MeV) reactions. The data points give statistical errors, and the solid lines are the $f(P_R)$ used in the Monte Carlo and TRIDIF codes.

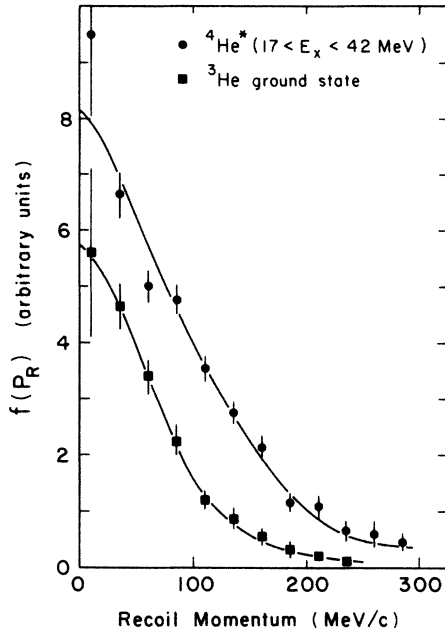


FIG. 7. The form factor, $f(P_R)$, in Eq. (2) for the ${}^6\text{Li}(\pi^+, \text{pd}){}^3\text{He}(\text{g.s.})$ and ${}^7\text{Li}(\pi^+, \text{pd}){}^4\text{He}(17 \rightarrow 42)$ reactions. The data points give statistical errors, and the solid lines are the $f(P_R)$ used in the Monte Carlo and TRIDIF codes.

form factors peak near 60 MeV/c indicating that the (pnn) nucleons removed from the target were in a state of total angular momentum $L=1$ in the target. The ${}^3\text{He}(5 \rightarrow 30 \text{ MeV})$ apparently also has an $L=0$ component as indicated by a sizable yield at zero recoil momentum, but this is uncertain because of the large statistical errors. The form factors for the ${}^6\text{Li}(\pi^+, \text{pd}){}^3\text{He}(\text{g.s.})$ and ${}^7\text{Li}(\pi^+, \text{pd}){}^4\text{He}(17 \rightarrow 42)$ in Fig. 7 are strongly peaked at zero recoil momentum indicating a dominant $L=0$ component and no noticeable $L=1$ component.

The shapes of the form factors for the ${}^3\text{He}(\text{g.s.})$ and ${}^4\text{He}(\text{g.s.})$ are close to what is expected using a "quasi-triton" cluster model for the (π^+, pd) reaction. The ${}^3\text{He}(\text{g.s.})$ form factor which we extracted from the data (Fig. 7) falls off to one-tenth its maximum value at about 150 MeV/c. This agrees with a measured ${}^6\text{Li}(\text{p}, \text{pt}){}^3\text{He}(\text{g.s.})$ triton knockout reaction where the recoil momentum distribution (corrected for phase space) also falls off to one-tenth at about 150 MeV/c.⁸ However, another ${}^6\text{Li}(\text{p}, \text{pt})$ experiment⁹ shows the recoil momentum distribution falling off to one-tenth at about 130 MeV/c.

The ${}^7\text{Li}(\pi^+, \text{pd}){}^4\text{He}(\text{g.s.})$ form factor (Fig. 6) is also in reasonable agreement with the knockout reactions. It peaks at about 60 MeV/c, falling off a factor of 2 at 0 MeV/c and a factor of 5 at 160 MeV/c. This compares well with the ${}^7\text{Li}(\text{p}, \alpha){}^3\text{H}$ measurement¹⁰ where the momentum distribution peaks at 55 MeV/c, falls off a factor of 2 at 0 MeV/c, and a factor of 5 at 140 MeV/c. Another experiment, ${}^7\text{Li}(\text{n}, \alpha)\text{n}$, shows¹¹ that the momentum distribution of tritons in ${}^7\text{Li}$ peaks at 60 MeV/c.

It is less clear, using the "quasi-triton" cluster model, what to expect for the excited state form factors. The

transitions to the excited state regions must involve the removal of at least one of the $(1s^4)$ core nucleons. If one or three are removed, one would expect an $L=0$ form factor. If two of the $(1s^4)$ nucleons are removed with one $1p$ nucleon, then an $L=1$ transition would occur. There is no noticeable $L=1$ strength in the ${}^4\text{He}^*(17 \rightarrow 42)$ region which is surprising. In fact the form factor for the ${}^7\text{Li}(\pi^+, \text{pd}){}^4\text{He}^*(17 \rightarrow 42)$ region appears to be depressed at 60 MeV/c (Fig. 7), the region where the $L=1$ strength should peak. This should be contrasted with the ${}^3\text{He}^*(5 \rightarrow 30)$ form factor in Fig. 6 showing a dominant $L=1$ strength. This difference between the ${}^3\text{He}^*(5 \rightarrow 30)$ and ${}^4\text{He}^*(17 \rightarrow 42)$ form factors appears to be much larger than the statistical uncertainty, but because this result is so unexpected it would be preferable to repeat the experiment with better statistics before reaching any definite conclusion. At large recoil momentum the ${}^3\text{He}^*(5 \rightarrow 30)$ and ${}^4\text{He}^*(17 \rightarrow 42)$ form factors are very similar, falling off much more gradually than the ground state transitions. For example, at 150 MeV/c the ${}^4\text{He}^*(17 \rightarrow 42)$ form factor has fallen to 30% of its peak value compared to a fall to 10% of the peak value for the ${}^3\text{He}(\text{g.s.})$ form factor. Similarly, at 200 MeV/c the ${}^3\text{He}^*(5 \rightarrow 30)$ form factor has fallen to 19% of its peak value compared to a fall below 5% of the peak value for the ${}^4\text{He}(\text{g.s.})$ form factor. This gradual fall of the excited state form factors is probably due primarily to the four-, five- and six-body continuum. We have also looked for the dependence of the T matrix on the direction of \mathbf{P}_R , as was done in our previous work on the $(\pi^+ \text{pp})$ reactions.^{2,5} In no case did we find any angular dependence outside of experimental error. Therefore our T matrix reduces to the simple form of Eq. (2). This is consistent with the "quasi-triton" model which treats the recoiling nucleons as spectators.

IV. CROSS SECTIONS AND ANGULAR DISTRIBUTIONS

Once the functional form and the magnitude of the T matrix for a particular (π^+, pd) transition is known, it can be used to calculate any single-, double-, or triple-differential cross section. A computer program, TRIDIF,^{2,5} was written for this purpose. Any triple-differential cross section calculated by TRIDIF within the phase space acceptance of the experiment is model independent to the extent that the T matrix used in TRIDIF was freely adjusted until it reproduced the data. Calculating any single- or double-differential cross section using TRIDIF, or a total-integrated cross section involves the extrapolation of the T matrix into unmeasured regions of phase space.

The T matrix, Eq. (2), is composed of a form factor and the angular function, $G(\theta'_p)$. The form factors were chosen as the solid lines in Figs. 6 and 7 and $G(\theta'_p)$ was chosen to be the measured ${}^3\text{H}(\pi^+, \text{p}){}^2\text{H}$ angular distribution in the center of mass of the $\text{p} + \text{d}$ system. This choice of $G(\theta'_p)$ is discussed below. With this choice triple-differential cross sections are calculated by TRIDIF and are shown in Fig. 8 for the proton laboratory angle of 60° . The deuteron angle was chosen to be the conjugate angle for $\theta_p = 60^\circ$ in the case of zero recoil momentum.

This conjugate angle depends weakly on the Q value for the reaction and varies between 103.4° and 104.7° for the four cases considered. For the $\theta_p=60^\circ$ data the deuteron detector was situated at 102.7° but scanned a region of 12° about this central value. The “experimental” points in Fig. 8 show the statistical errors from the data and the Monte Carlo simulation. These “data” points are

$$\text{“data” points} = \frac{\text{data events } (E_p)}{\text{Monte Carlo } (E_p)} \frac{d^3\sigma(\text{TRIDIF})}{d\Omega_p d\Omega_d dE_p}, \quad (3)$$

where the same T matrix was used in both the TRIDIF and the Monte Carlo code. The degree to which the TRIDIF calculation goes through the data points indicates how well the Monte Carlo code is reproducing the data. The proton energy distributions are well reproduced by the Monte Carlo simulation. Only the statistical errors are shown in Fig. 8.

Single-differential cross sections are obtained by integrating over dE_p and $d\Omega_d$. Only 15% to 20% of the single-differential cross section is contained within the phase space of the detectors, thereby requiring a sizable extrapolation. Much of the extrapolation into the unmeasured region involves a knowledge of $f(P_R)$ at large values of recoil momentum. We instituted a cutoff momentum of 200 MeV/ c above which, the $f(P_R)$ used in the TRIDIF code is set equal to zero. We did this for several reasons. First, there are very few counts in our ground state transitions above 200 MeV/ c . Second, the data are restricted to a very narrow range of θ_R and ϕ_R values at large recoil momentum making it difficult to verify accurately the assumption that the T matrix is isotropic in these variables. Third, the region above 200

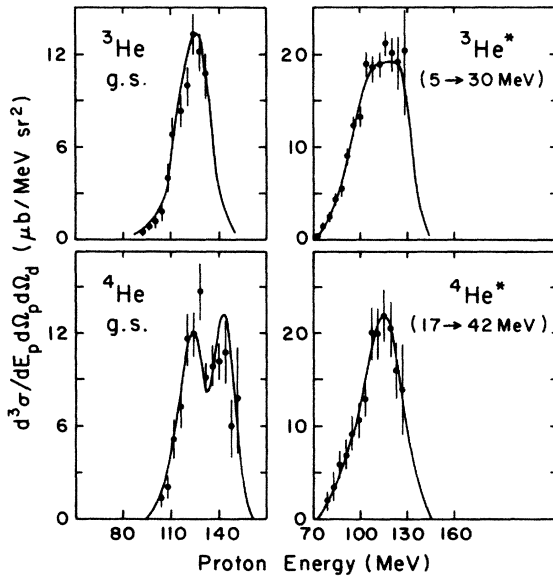


FIG. 8. The triple-differential, laboratory cross sections, $d^3\sigma/dE_p d\Omega_p d\Omega_d$ for the (π^+, pd) reactions to the states specified. The angle is 60° and the deuteron angle is the conjugate angle corresponding to zero recoil momentum. The solid lines are the TRIDIF calculation and the data points are Eq. (3) with statistical errors.

MeV/ c for the excited states is probably dominated by four-, five- and six-body final states. We are, of course, treating all of the undetected particles as a single entity with total momentum, P_R .

Limiting P_R to less than 200 MeV/ c , the TRIDIF code gives the single-differential cross sections in Table I. The three angles in Table I represent the three central angles of our proton detector during the experiment. The 60° and 102.7° data were taken simultaneously with the protons going into different detectors. To minimize the effect of $G(\theta'_p)$ upon the TRIDIF calculation of the single-differential cross sections, the T matrix was renormalized using the data yield at each proton angle. By doing this, the $G(\theta'_p)$ dependence in the T matrix will only change the extracted cross sections by a few percent. The sensitivity to $G(\theta'_p)$ is not totally eliminated because the proton detector scans a finite range of θ_p angles for each data set and there is not a one-to-one correspondence between θ_p , the proton laboratory angle, and θ'_p , the proton angle in the $p+d$ center-of-mass reference frame. The reason, of course, for renormalizing the T matrix for each data set is that we can examine the $G(\theta'_p)$ dependence to see if we made the correct choice for $G(\theta'_p)$. By examination of the single-differential cross section, we find that the present choice of $G(\theta'_p)$ works very well. This result is shown for the ${}^7\text{Li}(\pi^+, pd){}^4\text{He}$ ground state transition in Fig. 9 where we compare this angular distribution to the elementary ${}^3\text{H}(\pi^+, p){}^2\text{H}$ angular distribution¹² and find them to be identical in shape within experimental errors. The other three (π^+, pd) transitions with single-differential cross sections given in Table I are also in approximate agreement with the shape of the ${}^3\text{H}(\pi^+, p){}^2\text{H}$ angular distribution. Therefore we chose all four (π^+, pd) transitions to have the same $G(\theta'_p)$ dependence based upon the elementary ${}^3\text{H}(\pi^+, p){}^2\text{H}$ angular distribution.

If we repeated the TRIDIF calculation with a T matrix which is isotropic in θ'_p , then the largest change in our cross sections would be 2.5% increase in the $\theta'_p=60^\circ$ laboratory cross sections. Therefore our calculation does not depend strongly upon the choice of $G(\theta'_p)$. It is somewhat academic for us to include $G(\theta'_p)$ in our T matrix and we do it only to be consistent with the “quasi-triton” model.

The last thing to examine is the magnitude of the (π^+, pd) cross sections. In Fig. 9 it appears that the ${}^7\text{Li}(\pi^+, pd){}^4\text{He}(\text{g.s.})$ cross section is about 75% to 80% of the ${}^3\text{He}(\pi^+, p){}^2\text{H}$ cross section. However, it should be pointed out that an earlier measurement¹³ of the ${}^2\text{H}(p, \pi^+){}^3\text{H}$ reaction at $T=340$ MeV, gives by detailed balance a cross section for the ${}^3\text{H}(\pi^+, p){}^2\text{H}$ reaction at $T(\text{lab})=89$ MeV only half as large as the ${}^3\text{H}(\pi^+, p){}^2\text{H}$ cross

TABLE I. $d\sigma/d\Omega_p$ ($\mu\text{b}/\text{sr}$) for ${}^6,7\text{Li}(\pi^+, pd){}^3,4\text{He}$. For recoil momentum ≤ 200 MeV/ c .

Final state	$\theta_p =$	60	80.5	102.7
${}^4\text{He}(\text{g.s.})$		68.1 ± 6	27.7 ± 3	18.5 ± 2
${}^4\text{He}^* (17 \rightarrow 42)$		142 ± 10	45.5 ± 4	56.9 ± 5
${}^3\text{He}(\text{g.s.})$		37.2 ± 4		14.5 ± 2
${}^3\text{He}^* (5 \rightarrow 30)$		182 ± 14		71.4 ± 7

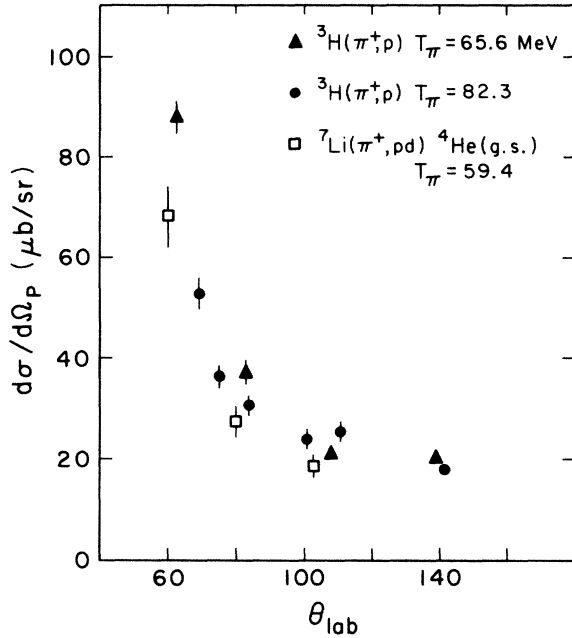


FIG. 9. The single-differential laboratory cross section $d\sigma/d\Omega_p$, of the ${}^3\text{H}(\pi^+, \text{p}){}^2\text{H}$ reaction deduced from Ref. 12 using detailed balance and compared to $d\sigma/d\Omega_p$ for the ${}^7\text{Li}(\pi^+, \text{pd}){}^4\text{He}(\text{g.s.})$ transition.

section¹² shown in Fig. 9. Furthermore, our measurements depend upon the accuracy of the ${}^2\text{H}(\pi^+, \text{p})$ cross sections and are subjected to a 10% systematic uncertainty in the normalization procedure. We conclude from this that within the experimental uncertainties the ${}^7\text{Li}(\pi^+, \text{pd}){}^4\text{He}(\text{g.s.})$ angular distribution is identical in both magnitude and shape with the elementary ${}^3\text{H}(\pi^+, \text{p}){}^2\text{H}$ reaction.

The ${}^6\text{Li}(\pi^+, \text{pd}){}^3\text{He}(\text{g.s.})$ cross section in Table I is about 60% of the ${}^7\text{Li}(\pi^+, \text{pd}){}^4\text{He}(\text{g.s.})$ cross section. This is approximately the fractional parentage of the ${}^6\text{Li}$ target split into ${}^3\text{He}$ and triton clusters.¹⁴ The ${}^7\text{Li}$ nucleus has a fractional parentage of about unity for a configuration with ${}^4\text{He}$ and triton clusters. Therefore, the ${}^7\text{Li}(\pi^+, \text{pd}){}^4\text{He}(\text{g.s.})$ and ${}^6\text{Li}(\pi^+, \text{pd}){}^3\text{He}(\text{g.s.})$ cross sections, relative to the elementary ${}^3\text{H}(\pi^+, \text{p}){}^2\text{H}$ cross section, scale according to the fractional parentage of the triton cluster in each target. This is further evidence that the (π^+, pd) reaction is occurring on a triton cluster.

Assuming that the full shape of the (π^+, pd) angular distributions is the same as the elementary ${}^3\text{H}(\pi^+, \text{p}){}^2\text{H}$ angular distribution from 0° to 180° , we can integrate over θ_p to get the total cross section. To find the full shape of the ${}^3\text{H}(\pi^+, \text{p}){}^2\text{H}$ angular distribution we use the data of Aslanides *et al.*¹⁵ from 7° to 59° and the data of Franz *et al.*¹⁶ from 140° to 175° and combine it with the data of Lolos *et al.*¹² from 68° to 144° . The integration gives the total cross sections as listed in Table II. The total (π^+, pd) cross section on both ${}^6\text{Li}$ and ${}^7\text{Li}$ is about 3 mb. This is about $8\frac{1}{2}$ percent of the total pion absorption cross section² on the lithium nuclei at $T_\pi = 59$ MeV. In extrapolating the (π^+, pd) yield to obtain the 3 mb total cross sec-

TABLE II. Total cross sections.

${}^4\text{He}(\text{g.s.})$	0.93 mb
${}^4\text{He} (17 \rightarrow 42)$	1.95 mb
${}^3\text{He}(\text{g.s.})$	0.56 mb
${}^3\text{He} (5 \rightarrow 30)$	2.48 mb

tion, we set the form factors to zero at a momentum cutoff of 200 MeV/c, as discussed above. By doing this we are eliminating 15% or more of the (π^+, pd) yield. Most of this ignored yield probably comes from four- and five-body final states which we cannot properly extrapolate. The integrated ${}^6\text{Li}(\pi^+, \text{pp})$ cross section takes about 60% of the total pion absorption cross section on ${}^6\text{Li}$ at 59 MeV or 20.4 mb so that the (π^+, pp) and (π^+, pd) channels account for about 70 percent of the total absorption cross section at this energy.

A recent stopped π^- on ${}^6\text{Li}$ experiment¹⁹ detected n, p, d, and t particle pairs. The four major channels nn, np, nd, and nt accounted for 97.4% of all particle pairs. The respective percentages for these four pairs were observed to be 72.5%, 7.1%, 12.0%, and 5.7%. No information was provided for converting these percentages to fractions of the total pion absorption cross section. The (π^-, nn) and (π^+, nd) channels are equivalent to the (π^+, pp) and (π^+, pd) channels by charge symmetry. The ratio of the total cross sections of ${}^6\text{Li}(\pi^+, \text{pd})$ and ${}^6\text{Li}(\pi^+, \text{pp})$ obtained by extrapolating our quasi-triton and quasi-deuteron T matrices, respectively, is 0.147. Correcting for the fraction of (π^+, pd) events above our cutoff momentum of 200 MeV/c, which were not included, we obtain a ratio of 0.17 which is nearly the same ratio, 0.16, as measured for the (π^-, nd) and (π^-, nn) events. The agreement of these ratios gives additional evidence that the quasi-triton model correctly describes the ${}^6\text{Li}(\pi^+, \text{pd})$ channel.

Because there is not available information on the absolute branching ratios of pion absorption on ${}^6\text{Li}$, it is interesting to look at stopped π^- on ${}^3\text{He}$ where such branching ratios exist. For ${}^3\text{He}$ it is found¹⁸ that 83% of the pion absorption cross section (not including pion charge exchange), goes into the nnp and nd channels. The remaining 17% involves the release of a high energy photon. As a comparison, the relative branching ratios measured in the stopped π^- on ${}^6\text{Li}$ experiment combined with our extrapolations of total cross sections, ${}^6\text{Li}(\pi^+, \text{pp})$ and ${}^6\text{Li}(\pi^+, \text{pd})$, suggests that about 83% of the total π^+ absorption cross section on ${}^6\text{Li}$ is attributable to particle pairs. Perhaps the remaining 17% is also due to the release of a high energy photon. This agreement with the ${}^3\text{He}$ data may be a chance coincidence, but nevertheless our extrapolations appear to be very consistent with other data.

V. CONCLUSIONS

The ${}^6,{}^7\text{Li}(\pi^+, \text{pd}){}^3,{}^4\text{He}$ reactions appear to be well described by a "quasi-triton" absorption model in which the pion interacts with and is absorbed on a "quasi-triton" cluster in the target. The evidence for this is fourfold. First, the shape of the form factors for the ground state transitions agree with the momentum distributions of

“quasi-tritons” measured in triton knockout reactions on the lithium nuclei. Second, the angular distributions of the (π^+,pd) transitions are the same as the elementary ${}^3\text{H}(\pi^+,p){}^2\text{H}$ reaction. Third, the magnitude of the ${}^3\text{He}$ and ${}^4\text{He}$ ground state transitions is approximately equal to the elementary ${}^3\text{H}(\pi^+,p){}^2\text{H}$ cross section times the known fractional parentage of each He ground state with a triton cluster in the target. Fourth, the T matrix for each transition can be described by Eq. (2), with no dependence upon the direction of the recoil momentum, \mathbf{P}_R .

There is one puzzling feature of the data which is not necessarily in contradiction with the quasi-triton model. The ${}^6\text{Li}(\pi^+,pd){}^3\text{He}^*$ ($5 \rightarrow 30$) form factor seems to show a strong $L=1$ shape indicating that two nucleons are removed from the $1s$ shell and one from the $1p$ shell. In contrast, the ${}^7\text{Li}(\pi^+,pd){}^4\text{He}^*$ ($17 \rightarrow 42$) does not show any $L=1$ strength indicating that either just one or all three nucleons are removed from the $1s$ shell. We have no ex-

planation for this difference.

Using the “quasi-triton” model to extrapolate our triple-differential cross sections into unmeasured regions of phase space, we can obtain estimates of about 3 mb for the total (π^+,pd) cross section on the lithium nuclei at 59.4 MeV. This represents about 8% of the total pion absorption cross section. Earlier we made a similar extrapolation of our ${}^6\text{Li}(\pi^+,pp)$ data using the quasi-deuteron model, obtaining a total cross section of 20.4 mb. The ratio of these extrapolated ${}^6\text{Li}(\pi^+,pd)$ and ${}^6\text{Li}(\pi^+,pp)$ cross sections is equal to the measured¹⁷ ratio for the charge symmetrical reactions, ${}^6\text{Li}(\pi^-,nd)$ and ${}^6\text{Li}(\pi^-,nn)$. This is additional evidence that the quasi-triton model provides a good description of the ${}^6\text{Li}(\pi^+,pd)$ reaction at $T=59.5$ MeV.

We are grateful to the staff at LAMPF for their full cooperation and readiness to meet our special needs.

*Permanent address: Physics Department, University of New Mexico, Albuquerque, NM 87131.

†Permanent address: Nuclear Physics Laboratory, University of Illinois, Champaign, IL 61820.

‡Permanent address: Brookhaven National Laboratory, Upton, NY 11973.

§Permanent address: American Scientist and Engineering, Inc., Cambridge, MA 02139.

**Present address: Lawrence Berkeley Laboratory, Berkeley, CA 94720.

¹J. P. Schiffer, *Comments Nucl. Part. Phys.* **14**, 15 (1985).

²R. Rieder, P. D. Barnes, B. Bassalleck, R. A. Eisenstein, G. Franklin, R. Grace, C. Maher, P. Pile, J. Szymanski, W. R. Wharton, F. Takeutchi, J. F. Amann, S. A. Dytman, and K. G. R. Doss, *Phys. Rev. C* **33**, 614 (1986).

³W. R. Wharton, in *Pion Production and Absorption—1982 (Indiana University Cyclotron Facility)*, Proceedings of Pion Production and Absorption in Nuclei, AIP Conf. Proc. No. 79, edited by R. D. Bent (AIP, New York, 1982), p. 371.

⁴P. D. Barnes, B. Bassalleck, R. A. Eisenstein, G. Franklin, R. Grace, C. Maher, P. Pile, R. Rieder, J. Szymanski, W. R. Wharton, J. R. Comfort, F. Takeutchi, J. F. Amann, S. Dytman, and K. G. R. Doss, *Nucl. Phys.* **A402**, 397 (1983).

⁵W. R. Wharton, P. D. Barnes, B. Bassalleck, R. A. Eisenstein, G. Franklin, R. Grace, C. Maher, P. Pile, R. Rieder, J. Szymanski, J. R. Comfort, F. Takeutchi, J. F. Amann, S. A. Dytman, and K. G. R. Doss, *Phys. Rev. C* **31**, 526 (1985).

⁶B. G. Ritchie, G. S. Blanpied, R. S. Moore, B. M. Preedom, K. Gotow, R. C. Minehart, J. Boswell, G. Das, H. J. Ziock, N. S. Chant, P. G. Roos, W. J. Burger, S. Gilad, and R. P.

Redwine, *Phys. Rev. C* **27**, 1685 (1983).

⁷W. K. Lin, F. Scheibling, and R. W. Kavanagh, *Phys. Rev. C* **1**, 816 (1970).

⁸W. Dollhopf, C. Lunke, C. F. Perdrisat, P. Kitching, W. C. Olsen, J. R. Priest, and W. K. Roberts, *Phys. Rev. C* **8**, 877 (1973).

⁹P. G. Roos, D. A. Goldberg, N. S. Chant, R. Woody, III, and W. Reichart, *Nucl. Phys.* **A257**, 317 (1976).

¹⁰M. Jain, P. G. Roos, H. C. Pugh, and H. D. Holmgren, *Nucl. Phys.* **A153**, 49 (1970).

¹¹B. Antolkovic, *Nucl. Phys.* **A219**, 332 (1974).

¹²G. J. Lolos, E. L. Mathie, G. Jones, E. G. Auld, G. Giles, B. McParland, P. L. Walden, W. Ziegler, and W. R. Falk, *Nucl. Phys.* **A386**, 477 (1982).

¹³W. J. Frank, K. C. Bandtel, R. Madey, and B. J. Moyer, *Phys. Rev.* **94**, 1716 (1954).

¹⁴F. Ajzenberg-Selove, *Nucl. Phys.* **A413**, 1 (1984).

¹⁵E. Aslanides, R. Bertini, O. Bing, F. Brochard, Ph. Goroetzky, F. Hibou, T. S. Bauer, R. Beurtey, A. Boudard, G. Bruge, H. Catz, A. Chaumeaux, P. Couvert, H. H. Duhm, D. Garreta, G. Igo, J. C. Lugol, M. Matoba, and Y. Terrien, *Phys. Rev. Lett.* **39**, 1654 (1977).

¹⁶J. Franz, H. P. Gortz, M. Kleinschmidt, L. Lehmann, P. Reichmann, E. Rössle, and H. Schmitt, *Phys. Rev. Lett.* **93B**, 384 (1980).

¹⁷M. Dorr, W. Fetscher, D. Gotta, J. Reich, H. Ullrich, G. Backenstoss, W. Kowald, and H.-J. Weyer, *Nucl. Phys.* **A445**, 737 (1985).

¹⁸P. Truöl, H. W. Baer, J. A. Bistirlich, K. M. Crowe, N. deBotton, and J. A. Helland, *Phys. Rev. Lett.* **32**, 1268 (1974).